Critical Issues in Hydrogen Assisted Cracking of Structural Alloys

Richard P. Gangloff

R.P. Gangloff, "Critical Issues in Hydrogen Assisted Cracking of Structural Alloys", in Environment Induced Cracking of Metals (EICM-2), Sergei Shipilov, ed., Elsevier Science, Oxford, UK, in press (2006).

Critical Issues in Hydrogen Assisted Cracking of Structural Alloys

Richard P. Gangloff

Department of Materials Science and Engineering, University of Virginia, Charlottesville, VA 22903-2442, USA

Abstract

Both internal and hydrogen environment assisted cracking continue to seriously limit high performance structural alloys and confound quantitative component prognosis. While intergranular H cracking assisted by impurity segregation can be minimized, other mechanisms promote IG cracking and transgranular H cracking modes have emerged; new alloys suffer serious H cracking similar to old materials. Micromechanical models of crack tip H localization and damage by decohesion predict important trends in threshold and subcritical crack growth rate behaviour. H diffusion appears to limit rates of cracking for monotonic and cyclic loading; however, uncertain-adjustable parameters hinder model effectiveness. It is necessary to better define conditions within 0.1-5 μm of the crack tip, where dislocations and microstructure dominate continuum mechanics, and chemistry is localized. Nano-mechanics modeling and experimental results show very high levels of H accumulated in the crack tip fracture process zone, as necessary for interface decohesion. Contributing mechanisms include high crack tip stresses due to dislocation processes such as strain gradient plasticity, as well as powerful H production and trapping proximate to the electrochemically reacting crack tip surface. New sub-micrometer resolution probes of crack tip damage will better define features such as crack path crystallography (EBSD + Stereology) and surface morphology (high brightness, dual detector SEM), local H concentration (TDS and NRA), and validate crack tip mechanics modelling (micro-Laue x-ray diffraction and EBSD).

Keywords: (A) alloy, (B) modelling studies, (C) hydrogen embrittlement, (C) corrosion fatigue, (C) stress corrosion

1. Introduction

Both internal hydrogen assisted cracking (IHAC) and hydrogen environment assisted cracking (HEAC) limit the performance of most modern structural alloys, and confound prognosis of component safety, durability and capability. Figure 1 demonstrates that subcritical IHAC and HEAC occur at threshold stress intensity (K_{TH}) levels well below

plane strain fracture toughness, K_{IC}, for modern Ti alloys and ultra-high strength steels subjected to quasi-static loading. IHAC and HEAC occur at similarly low K_{TH} (shaded areas) and are governed by important variables of alloy composition and yield strength, heat treatment and microstructure, applied K level and application rate, temperature, and hydrogen concentration. IHAC and HEAC are severe in precipitation hardened Al and Ni alloys, and the damaging effect of atomic hydrogen (H) is exacerbated in most materials by cyclic loading.

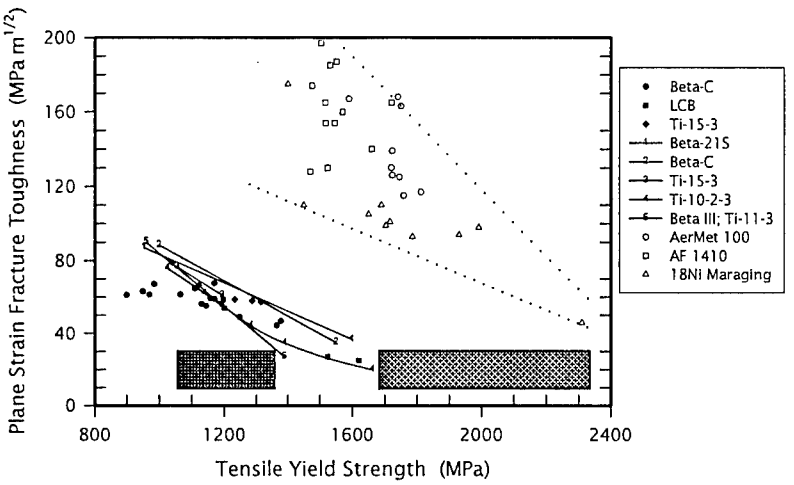

Figure 1. Yield strength dependence of K_{IC} for high strength α-precipitation hardened β-Ti alloys and ultra-high strength tempered martensitic alloy steels. Shaded areas represent lower bound K_{TH} regimes for IHAC and HEAC in these structural alloys.

In response a massive literature has developed; particularly a proceedings on hydrogen and stress corrosion cracking in iron alloys [1], the first International Conference on Environment-Induced Cracking of Metals [2], 6 conferences on hydrogen effects in metals [e.g., 3], a dedicated journal volume [4], and recent reviews of subcritical H-assisted crack growth under quasi-static loading [5] and fatigue deformation [6,7].

The objective of this review is to present recent results and suggest new approaches relevant to the persisting uncertainties that hinder: (a) understanding of hydrogen damage physics and the role of H in environment assisted cracking, (b) alloy development for H cracking control, and (c) mechanism-based models of material subcritical crack growth kinetics for use in component prognosis.

2. Hydrogen Damage Mechanisms

Two mechanistic issues dominated scientific discussion over the past several decades.

What is the basic mechanism for hydrogen damage leading to subcritical crack growth when brittle hydride does not precipitate?

Does the HEAC mechanism explain environment-assisted (stress corrosion) crack growth in high strength alloys stressed in moist environments?

Candidate damage mechanisms; Hydrogen Enhanced Bond Decohesion, Hydrogen Enhanced Localized Plasticity, and Adsorption Induced Dislocation Emission; are reviewed elsewhere [5,8-11]. Arguments supporting each are not definitive, but a consensus is emerging that H-reduced bond strength is the mechanism for cracking of Fe, Ti, Al and Ni alloys. This view is strong for interface cracking, while plasticity may play a role in slip band and crystallographic cracking. Decohesion is suggested by high magnification examination of intergranular surfaces (see Section 5), as well as modelling and experimental evidence of H enrichment in the crack tip fracture process zone (FPZ); Sections 4 and 5. Neither observations nor modeling establish a role for H-affected plasticity damage in complex microstructures. Slip about a crack tip has not been characterized to show H stimulated dislocation emission and crack extension. High strength alloys contain an array of finely spaced barriers to dislocations that should provide back-stress to stifle dislocation emission and act as preferred traps to strip H from dislocations. The argument that only dislocation-based processes explain rapid rates of subcritical crack growth is refuted by analysis of H diffusion about a crack tip (Section 4). Micromechanical modeling of K_{TH} and growth rate (da/dt) for subcritical IHAC and HEAC has focused on decohesion, while H-stimulated plasticity has not been incorporated into testable models of macroscopic cracking kinetics.

Controversy has centered on the extent to which H damage explains subcritical crack growth in alloys stressed in environments that support concurrent crack tip dissolution, passive film formation, and atomic hydrogen production. A consensus has emerged that H provides the dominant damage mechanism for high strength alloys stressed in moist environments [5]. A critical element of this conclusion is modeling and measurement to predict the amount of H produced on occluded crack surfaces. Figure 2 shows such a result, where K_{TH} declines systematically with increasing amount of H absorbed on the crack tip surface in precipitation hardened nickel based superalloys [12,13].[1] A single correlation describes cracking in H_2 and acidic chloride solution, and the crack path varied from transgranular (TG) slip-band based to intergranular (IG) with increasing H content for each environment. These results support HEAC. Additional support was provided by measurements and modeling that explained the effect of applied electrode potential on da/dt in aluminum alloys stressed in acidified chloride [14]. Increased da/dt, in response to anodic and cathodic polarization, correlated to increased crack uptake of H measured by thermal desorption spectroscopy. Crack electrochemistry, and the use of applied electrode potential as a probe of cracking mechanism, are detailed elsewhere [5,16].

Additional debate on these issues will undoubtedly occur at this meeting [9].

3. Alloy Development for H-Cracking Resistance

The question is: *Can metallurgical advances in high strength and fracture toughness be extended to develop structural alloys that resist H cracking?* Recent results show that this goal remains elusive. Intergranular H cracking is mitigated by reduced impurity segregation [10,17], but other grain boundary damage mechanisms exist, TG

[1] The calculation in Fig. 2 included H crack chemistry change for the acid, but not potential decrease from the boldly exposed surface to the crack tip; and included H trapping at microstructural sites, but not enhancement due to hydrostatic stress. These factors should not alter comparison between the gas and electrolyte environments, but affect absolute H content.

H cracking modes have emerged, and causal microscopic factors are not understood. As such, new alloys suffer severe H cracking similar to older materials; strength and toughness gains from decades of research are compromised by H cracking.

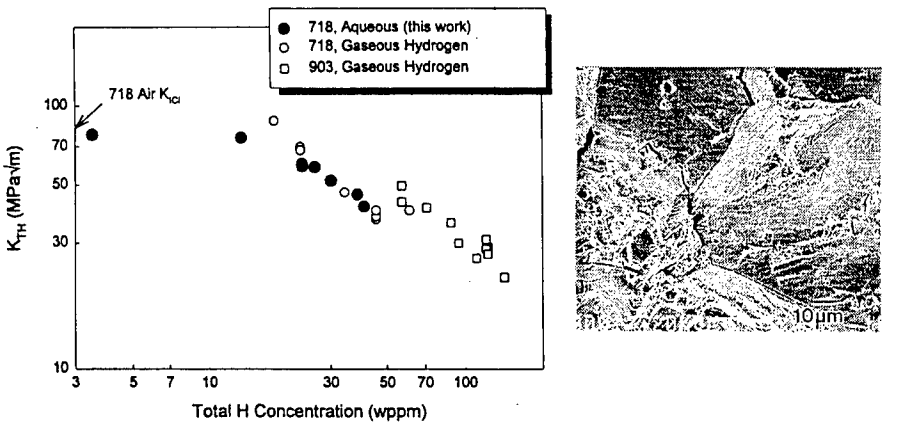

Figure 2. Threshold stress intensity for HEAC in peak aged IN718 and IN903, stressed in high pressure H_2 (9, O) or acidified chloride solution with cathodic polarization (•), *vs.* calculated H content produced at the crack tip. H-free superalloys cracked by microvoid processes at high K_{IC}, while HEAC in each environment produced mixed IG and TG slip-plane based cracking, as shown in the SEM fractograph (IN718 at K = 53 MPa√m) [12].

Severe HEAC and IHAC are produced in modern hcp-α precipitation hardened bcc β-Ti alloys, as shown in Figs. 3 [18,19] and 4 [20]. In each case H cracking depended on the rate of applied K (dK/dt) and required a critical amount of aging time and/or α precipitation. Experiments implicated grain boundary segregation for the IG HEAC in Fig. 3, rather than α precipitation [21]. However, no segregant was resolved by analytical electron microscopy and the fundamental cause of IG H cracking was not established. The TG IHAC in Fig. 4 is along α precipitate interfaces, formed in the Widmanstatten orientation on 4 variants of {111} in β. Hydrogen trapping at these interfaces likely explains this TG cracking and the aging dependence suggests a critical amount of α plate interface is required to form a connected path in β [20].

The IHAC in a modern tough and ultra-high strength steel (AerMet®100) is severe, Fig. 5, with K_{TH} as low as 10% of the H-free K_{IC} [22]. While dramatic at lower dK/dt, reduction in toughness persists to the highest loading rates studied (2000 MPa√m/s). This steel is not susceptible to IG H cracking, due to high purity that reduced elemental segregation to austenite grain boundaries [10,17]. Rather, cracking at low dK/dt is along interfaces in the lath martensite microstructure, while reduced toughness at higher loading rates correlates to microvoid-based cracking, with reduced void size due to predissolved H. Severe IHAC at the lower dK/dt was explained based on redistribution of H from a high density of low-binding energy trap sites at coherent M_2C carbides to martensite lath interfaces under high crack tip hydrostatic stresses [23]. As detailed in Section 5, this amount of trapped H can be estimated and model correlated to K_{TH} [23]. Metallurgical alteration to reduce M_2C coherence, and raise H-trap binding energy to

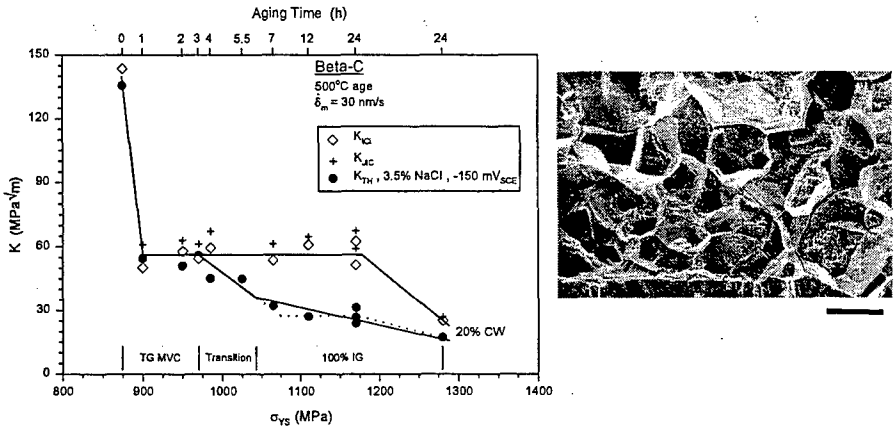

Figure 3. Strength and aging time dependencies of fracture toughness and K_{TH} for the onset of HEAC in solution treated Beta-C (Ti-3Al-8V-6Cr-4Mo-4Zr) stressed under slow-rising CMOD (δ_m) in moist air and aqueous-chloride solution at constant applied electrode potential of –150 mV_{SCE} and 25°C. The highest strength and lowest cracking resistance were achieved by 20% cold work (CW) prior to aging. The SEM fractograph shows the morphology of 100% intergranular HEAC for the 6 to 24 h age cases (100 μm bar).

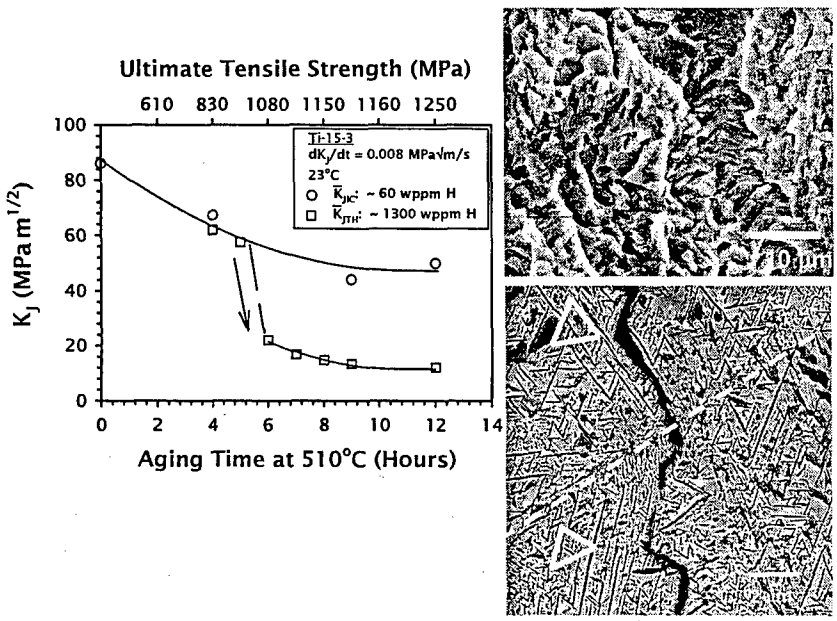

Figure 4. The aging time and yield strength dependencies of plane strain fracture toughness at the as-processed H content of 60 ppm and K_{TH} for IHAC in H-precharged ($C_{H\text{-}TOT}$ = 1300 wppm) Ti-15V-3Al-3Sn stressed in moist air at 25°C. The SEM fractograph (top) shows TG IHAC for the 12 h age case and metallographic cross-section (Bottom) shows that H-cracking progresses along β/α interfaces, with the α needles (dark phase) present in three variants on {111} in β shown by the triangles on either side of a high angle grain boundary (dashed line). The subscript, J, denotes elastic K calculated from the elastic-plastic J-integral, and the bar indicates the average of 1st initiation and blunting-line offset definitions of crack growth [20].

retard crack tip H repartition, should reduce IHAC. This hypothesis has not been tested. This steel is susceptible to severe TG HEAC in chloride solution [5].

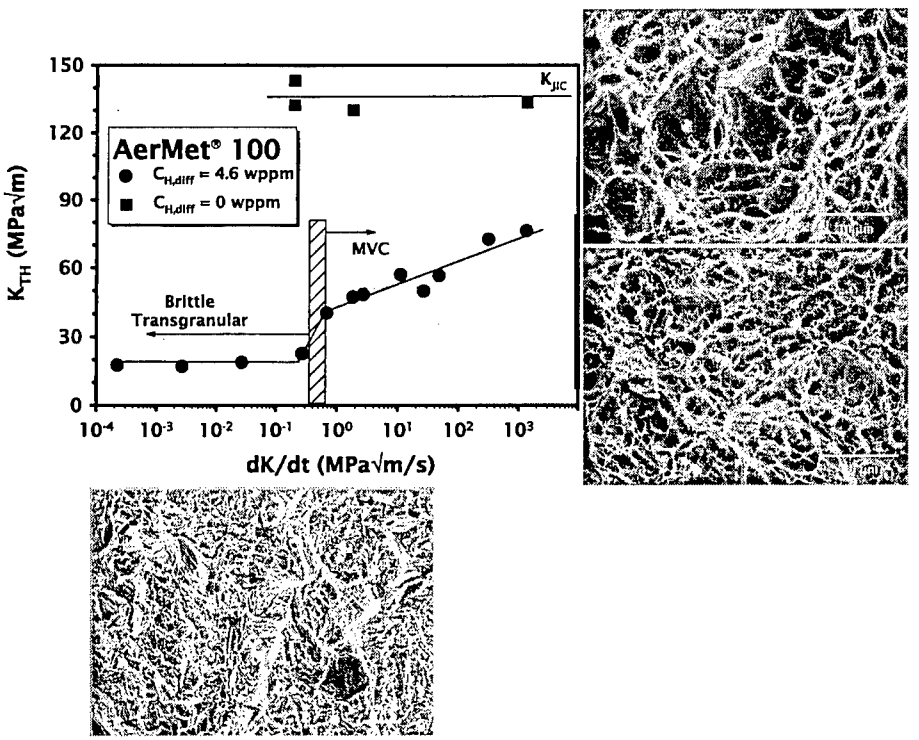

Figure 5. Rising CMOD K_{TH} *vs.* applied-initial dK/dt for AerMet®100 steel precharged to a diffusible H content ($C_{H\text{-}DIFF}$) of 4.6 wppm. At dK/dt less than 0.3 MPa√ms, brittle-TG fracture occurs at K_{TH} < 20 MPa√m. At dK/dt greater than 0.7 MPa√m/s, fracture is by microvoid processes. The H-free K_{IC} of AerMet®100 is ~135 MPa√m [22].

A modern α/β-Ti alloy and precipitation hardened 7000-series aluminum are susceptible to severe HEAC in H producing chloride solutions; Figs. 6 and 7 [24,25]. Both alloys were investigated for thermomechanical processing and aging developed for optimal yield strength and fracture toughness, not considering H cracking. The TG cracking in Ti-6-22-22 correlated with dislocation shearing of fine Ti_3Al (α_2) precipitates, analogous to the behavior of older α/β alloys [26,27]. The K_{TH} declined monotonically with increasing slip step height, as shown in Fig. 8 for the slip morphology in Fig. 6 [28]. Overaging for particle coarsening to block α_2 shearing and reduce HEAC was unsuccessful; 175 h aging at high temperature (593°C) produced severe slip band localization. Compositional modification can eliminate this phase, as known for decades, but novel metallurgical routes involving a second population of hard particles should be pursued to retain high strength.

While the beneficial effect of modest overaging in retarding IG HEAC in 7000-series aluminum alloys is well known and exploited in technology [29], Fig. 7, the

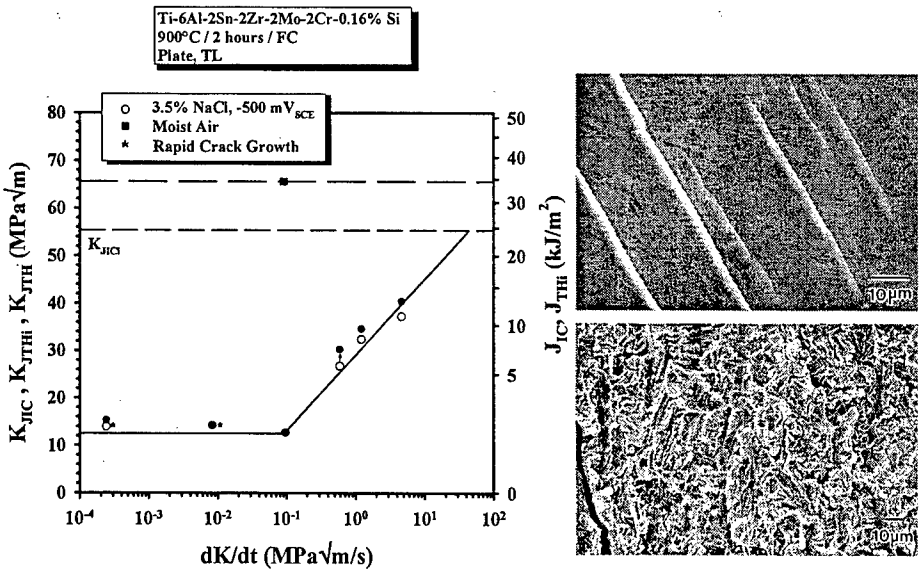

Figure 6. Loading rate dependence of K_{TH} for HEAC in Ti-6-22-22 plate stressed under rising K in aqueous NaCl solution. Cracking is TG as shown by the SEM image (lower right) and traced to highly localized planar slip from sheared Ti_3Al precipitates, as shown by the SEM image of a polished and deformed surface (top right) [24].

specific manifestation of aging that reduces H damage is not established [30]. Understanding is hindered because multiple microstructural variables change with aging time (e.g., boundary composition and precipitate size/spacing/composition, as well as intragranular precipitation, slip mode and PFZ characteristics). The causal factors are likely nano-scale and highly gradated in the vicinity of the crack tip along high angle grain boundaries, thus complicating structure and damage probes. The goal in this material class is to retain the strength of a peak aged microstructure and achieve immunity to HEAC. Better fundamental understanding of the aging effect is necessary.

4. Continuum Fracture Mechanics Modelling

The question is: *Can effective models of H-cracking kinetics be developed, based on fundamental decohesion or plasticity damage mechanisms, for use in next generation quantitative component life prediction and prognosis methods?*

The continuum fracture mechanics framework exists for macroscopic predictions of component subcritical crack growth in hydrogen service [31]. Major advances have been achieved in life prediction programs such as NASGRO (*http://www.nasgro.swri.org*), AFGROW (*http://afgrow.wpafb.af.mil*), and REACT (*http://www.srt-boulder.com*). For next generation prognosis, experimental cracking threshold and growth rate databases must be extended by models based on fundamental principles [32]. Micromechanical models of stress intensity thresholds and growth rates for IHAC and HEAC exist, but contain multiple-adjustable parameters due to persisting uncertainties, as reviewed in detail elsewhere [33-36].

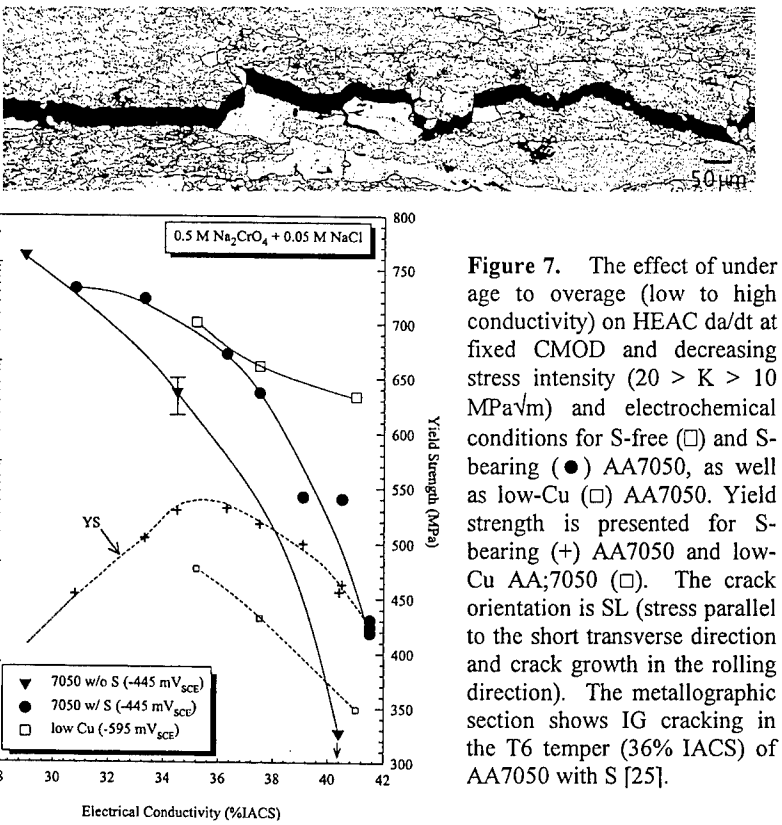

Figure 7. The effect of under age to overage (low to high conductivity) on HEAC da/dt at fixed CMOD and decreasing stress intensity (20 > K > 10 MPa√m) and electrochemical conditions for S-free (□) and S-bearing (●) AA7050, as well as low-Cu (□) AA7050. Yield strength is presented for S-bearing (+) AA7050 and low-Cu AA;7050 (□). The crack orientation is SL (stress parallel to the short transverse direction and crack growth in the rolling direction). The metallographic section shows IG cracking in the T6 temper (36% IACS) of AA7050 with S [25].

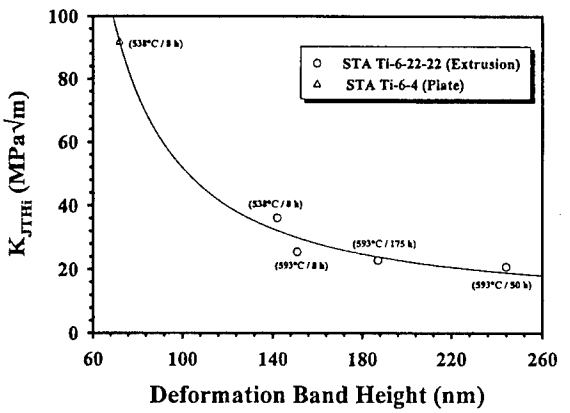

Figure 8. The effect of slip step height, from a polished-strained surface and varied by aging (temperature/time) to affect the size of Ti_3Al precipitates, on K_{TH} for two α/β titanium alloys stressed under slow-rising K in NaCl solution; Fig. 6 [28].

Two recent examples are presented, based on the hypothesis that subcritical crack growth rate is limited by H diffusion from crack tip H uptake sites to a critical distance, χ_{CRIT}, within the FPZ where H damage forms. In a large body of literature, the K-independent Stage II crack growth rate, da/dt_{II}, is modeled as the ratio of χ_{CRIT} to the time for H diffusion over this distance to reach a critical level, C_{CRIT}, relative to a crack tip surface H content of C_S [35]. Models are of varying complexity depending on whether the H-diffusion field is: (a) concentration and/or stress driven, (b) transient or

steady state, (c) ahead of a stationary or moving crack, (d) modeled in one or two dimensions, (e) emanating from environment-sensitive C_S, (f) microstructure-trap affected, (g) plastic strain-trap affected, and (h) coupled with a H-failure criterion. The results of this 1-dimensional modeling are of the form [35]:

$$\frac{da}{dt_{II}} = \frac{D_H}{\chi_{CRIT}}\left[\xi\left(\frac{C_s}{C_{CRIT}}, D_H, \chi_{CRIT}, \sigma_{YS}, t\right)\right] \quad (1)$$

where ξ is a function of the indicated variables and is 0.01-3.0 depending on the details in (a) through (h).

A large amount of experimental data on the relationship between da/dt_{II} and H-trap sensitive diffusivity, $D_{H\text{-}eff}$, is plotted in Fig. 9. Hydrogen diffusion control of HEAC is supported by the observed and predicted proportionality between da/dt_{II} and $D_{H\text{-}eff}$. The highest-reasonable value of ξ is 3 giving an χ_{CRIT} of 0.7 μm from the trend line in Fig. 9, independent of alloy. Smaller ξ result in smaller χ_{CRIT}. The results for gaseous-H producing environments are separate from those for electrolytes, as explained speculatively based on reduced $D_{H\text{-}eff}$ due to vacancy trapping of H, where vacancies are produced at crack tip surfaces by dissolution during cathodic H production [35]. This trend suggests that the χ_{CRIT} is nm-scale, even for low da/dt_{II} situations. While this result suggests that H diffusion rate limits da/dt_{II} for a range of HEAC situations, uncertain-adjustable parameters limit model effectiveness.

Hydrogen diffusion from surface reaction sites to locations of damage in the crack tip FPZ was proposed to rate limit environment enhanced fatigue crack propagation by HEAC [36]. If H diffusion is rate limiting, rather than mass transport in the environment or crack surface (electro)chemical reaction [37], then a 1-dimensional model predicts that the fastest (or plateau) rate of HEAC (da/dN_{CRIT}) occurs for all cyclic loading frequencies (f) less than a critical value (f_{CRIT}) given by:

$$\frac{da}{dN_{CRIT}} = \Delta a^* f_{CRIT} = 2\sqrt{\frac{D_H}{f_{CRIT}}}\,erf^{-1}\left(1-\frac{C_{CRIT}}{C_S}\right) \quad (2)$$

where the terms are as defined with regard to Eq. 1. In this model, a H-enhanced increment of crack growth occurs instantaneously at K_{MAX} in each fatigue cycle. Hydrogen production, diffusion, and discontinuous crack growth repeat between the present and next K_{MAX}, with the time between successive crack growth increments given by $1/f$. The maximum increment of crack growth, Δa^*, is determined by the location of maximum tensile stress ahead of the crack tip as controlled by K_{MAX}. In the plateau, loading time per cycle is sufficiently slow to enable H diffusion over the whole of Δa^*. Above f_{CRIT}, per-cycle time is insufficient to achieve C_{CRIT} over this distance and the amount of crack extension per cycle, or da/dN, is reduced. Extensive data for 7000-series alloys show that $da/dN_{CRIT} \propto 1/\sqrt{f}$, however, the values of $D_{H\text{-}eff}$, C_{CRIT} and C_S in Eq. 2 are uncertain and the model is not quantitatively predictive.

Hydrogen diffusion control of da/dN provides a unique description of HEAC for fatigue of aluminum alloys in pure water vapor and NaCl solution [36]. In Fig. 10, da/dN measured at a single stress intensity range, ΔK, is plotted as a function of an environmental exposure parameter. For fatigue in water vapor, this parameter is the

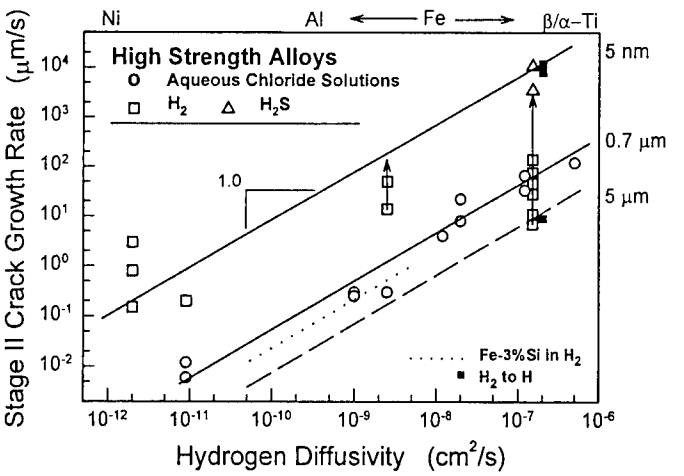

Figure 9. The dependence of da/dt_{II} on trap sensitive $D_{H\text{-}eff}$ for high strength alloys that exhibit HEAC in gases and electrolytes at 25°C. High strength austenitic stainless steel and nickel superalloys were cracked in high pressure (100–200 MPa) H_2, while maraging and tempered-martensitic steels were cracked in low pressure (~100 kPa) H_2. The dotted line represents TG cracking of Fe-3%Si single crystal in 100 kPa H_2 at 0°C to 125°C. Filled symbols (□) represent the transition from molecular to atomic hydrogen gas [35].

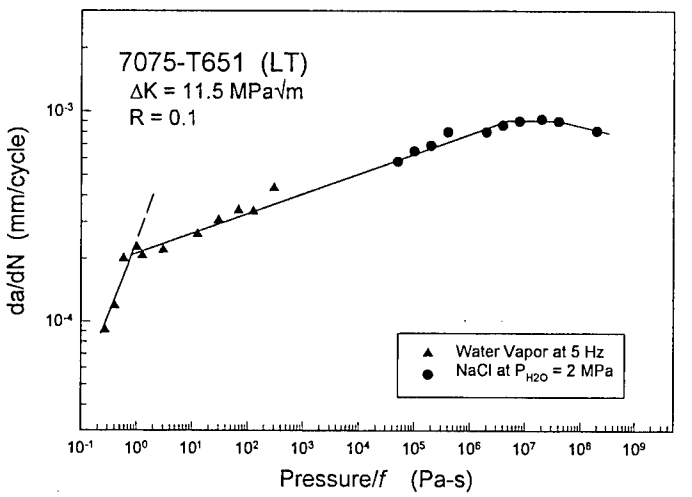

Figure 10. Fatigue crack growth rate for AA7075 in water vapor and NaCl solution *vs.* environmental exposure given by water vapor pressure/loading frequency. Results for NaCl (□) were positioned to provide a best fit with the water vapor data, assuming an effective H pressure of 2 MPa [36].

ratio of water vapor pressure to loading frequency [36,37]. The parameter for electrolytes is problematic due to uncertain crack H production. In Fig. 10, da/dN for NaCl are shifted along the exposure axis for a best fit with water vapor data using an

effective "pressure" of 2 MPa. This correlation suggests that da/dN is rate-limited by molecular transport at low P_{H2O}/f, surface reactions are rapid and produce increasing coverage of H through the oxidation of Al, and the da/dN *vs* exposure trend is represented by the steep-solid line [37]. The transition from this behavior is ascribed to da/dN limited by H diffusion in the FPZ [36]. A single line fits all data, suggesting that process zone H diffusion is rate-controlling for water vapor at intermediate to high pressures, as well as aqueous-chloride solution. The plateau at high environmental exposure is described by Eq. 2 and the subsequent falloff in da/dN is caused by corrosion-product induced crack closure promoted at very long per-cycle exposure times. While the correlation in Fig. 10 is interesting, a critical uncertainty remains; that is, the amount of H produced on crack tip surfaces during HEAC.

5. New Directions in Modelling and Measurement for H Cracking

The question is: *Can new solid mechanics and experimental developments be exploited to achieve breakthroughs in understanding and modeling hydrogen cracking?* Strong gradients in H concentration and stress about the crack tip govern crack growth in IHAC and HEAC, and challenge modeling and H-damage characterization necessary to develop next generation crack growth models and resistant alloys [5]. There is need for improved understanding of:

- Concentration of H absorbed on crack tip surfaces and dissolved in the crack tip FPZ, 0.05 to 5 μm ahead of the crack tip surface.
- Crack tip stresses within 0.05 to 5 μm of the crack tip, as affected by novel H-plasticity interaction and dislocation processes.
- High resolution determinations of crack morphology, crystallography, and FPZ hydrogen content.
- Effect of active monotonic and cyclic plastic strain on H cracking.

5.1 Crack Tip Hydrogen Enrichment

Hydrogen is enriched in the crack tip FPZ ($C_{H\text{-}FPZ\ trap}$) by 3 mechanisms: (a) crack surface accumulation at C_S by electrochemical processes, (b) high hydrostatic tension (σ_H) that dilates the lattice, and (c) segregation at trap sites with a binding energy, E_B. This enrichment is described approximately by:

$$\left(C_{H-FPZ\ trap}\right) = C_s \exp\left(\frac{E_B + \left(\sigma_H V_H\right)}{RT}\right) \tag{3}$$

where V_H is the partial molar volume of H in the host lattice [5]. Trap sites are typically interfaces and boundaries that constitute a connected path for brittle H-cracking. High values of C_S, σ_H and E_B promote H enrichment to exacerbate IHAC and HEAC. Emerging results support the notion that very high levels of crack tip H are accumulated, as likely necessary for the decohesion mechanism to be reasonable [38].

5.1.1 Stress and H Trapping Enrichment

The presence of very large stresses in the sub-micron crack tip FPZ is a requisite for hydrogen embrittlement, as recognized qualitatively by Oriani [38]. The reason is the need to raise low lattice and trapped concentrations of H at crack nucleation sites to justify lowering cohesive strength of the lattice or interface. It is critical to define the stress distribution about the H-affected crack tip, with emphasis on the mechanics over a sub-micrometer length scale. Classic continuum fracture mechanics formulations of blunt-crack tip stress and plastic strain distributions, J_2 in Fig. 11, predict that opening direction tensile (σ_{YY}) and hydrostatic stresses are (3-5)σ_{YS} dependent on alloy work hardening. These descriptions are inadequate for the next generation of material-behavior model building [39]. It is necessary to refine such predictions within 0.1 - 10 μm of the crack tip surface, considering dissolved H and for the length scale where dislocations and microstructure dominate continuum mechanics. Guidance is provided by important studies of H-free cleavage fracture in the presence of plastic deformation.

Each of several approaches show that stresses are larger than the blunted crack solution, using dislocation distributions that alter the near tip field. For an atomistically sharp IG crack tip, Thompson and then Kameda [40] invoked a dislocation-free zone between the crack tip and dislocation pile-up; σ_{YY} in this zone equaled (4-7)σ_{YS} at applied K typical of hydrogen cracking thresholds and joined the HRR field at the outer edge. Gerberich and coworkers modeled interaction of a distribution of dislocations that dominate very-near tip stresses and a superdislocation (removed from the tip) that defines global crack tip plasticity with work hardening [34,41]. The near-tip dislocations produce a constant sliding stress along the dislocation pile-up, canceling the crack tip singularity and producing a stress field with $\sigma_H \sim$ (30-50)σ_{YS}, maximized 20 nm ahead of a sharp crack tip [42]. Lipkin *et al.* note that if the rate of strain hardening exceeds the divergence of the stress field, material can no longer deform plastically. This is guaranteed by a large strain gradient that requires geometrically necessary dislocations (GND)and increased hardening [43]. The size of the resulting elastic core is determined by stress continuity with the HRR field. Calculations with material properties used for the J_2 curve in Fig. 11 place the size of the elastic core at ~250 nm (or 0.25l), and predict significant stress elevation over the J_2 results.

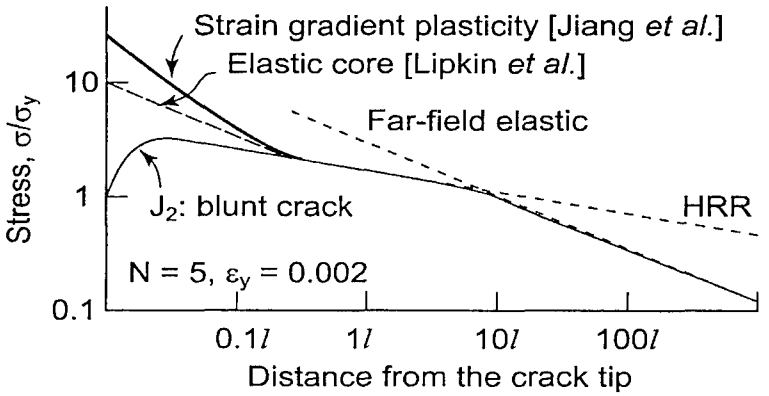

Figure 11. Crack tip stress distributions from various modeling approaches and normalized to a material-based length, l, that is of order 1 μm [44]. (σ_Y is flow stress, ~σ_{YS}, and σ is σ_{YY}.)

The GND concept provides a related explanation for enhanced crack tip stresses [45,46]. A finite density of GND accommodate a large strain gradient, implying that strain hardening is exacerbated at a crack tip where a gradient is implicit and broad-scale plasticity from blunting is limited. Hydrogen cracking at low K provides such a situation. An intrinsic material length scale controls the contribution of a strain gradient to Taylor-based strain hardening. This length scale is a phenomenological constant that relates to microstructure [46], or is connected analytically to specific dislocation interactions [47]. The curve in Fig. 11 depicts the σ_{YY} distribution derived from incorporating strain gradient terms into the material hardening description [47]. The length scale of the stress elevation is controlled by the material length scale, l; this parameter was inferred to be 0.5-5 μm from micro-indentation and wire torsion experiments applied to model single phase metals [46]. For comparison with dislocation-based models, it is convenient to assume l = 1 μm in Fig. 11. For this case, it is clear that the strain gradient is large enough to significantly alter the HRR field over ~ 300 nm. The location of the maximum stress in a gradient-affected fracture is not clear, since only asymptotically sharp cracks have been modeled.

Discrete dislocation dynamics simulations support these explicit treatments of near tip dislocations and enhanced hardening due to a strain gradient [48]. The near-tip fields resulting from simulation reveal many of the characteristics obtained via continuum models that invoke a priori assumptions of dislocation behavior: (i) crack tip openings remain sharp, (ii) near tip stresses are significantly higher than those predicted by plasticity models without reference to microstructure, (iii) a dislocation free zone can arise near the crack tip, and (iv) crack tip shielding is a function of the density of dislocation nucleation sources. Quantitative comparison of maximum stresses at the crack tip with the models in Fig. 11 is not feasible due to the inclusion of a cohesive zone fracture element at finite critical stress.

A recent investigation of IHAC in ultra-high strength AerMet®100 steel demonstrates the role of crack tip stress in promoting H accumulation and embrittlement. The cracking threshold data in Fig. 5 were determined for a constant diffusible H content ($C_{H\text{-}diff}$) of 4.6 wppm [22]. The low-dK/dt K_{TH} level decreased monotonically with rising $C_{H\text{-}diff}$ from 0.5 to 8 wppm. Cracking was along martensite lath-interface microstructure, as illustrated in Fig. 5. The explanation for the cause of this severe IHAC is provided by the comparison in Fig. 12. Hydrogen repartitions from a lower binding energy trap state, in this case nano-scale M_2C with a coherent interface and E_B ~12 kJ/mol, to the crack tip and martensitic interfaces when the stress-interaction energy ($\sigma_H V_H$) > E_B for the source trap. The calculation in Fig. 12 (left) shows that this happens for AerMet®100 (σ_{YS} = 1760 MPa) when the ratio of σ_H/σ_{YS} > 3.0. The probability that this repartition of H occurs rises as the difference between E_B and $\sigma_H V_H$ increases, demonstrating that IHAC is exacerbated by increased crack tip stresses. For example, the probability that H repartitions from M_2C interfaces to lattice sites acted on by σ_H is 0.22 when σ_H is $2.5\sigma_{YS}$, 0.92 when σ_H is $5.0\sigma_{YS}$ and 0.998 when σ_H is $8.0\sigma_{YS}$, each for an M_2C binding energy of E_B = 12 kJ/mol [23,49,50].

The combined effects of interface trapping and hydrostatic stress on enhancing the concentration of H in the FPZ are dramatic. For a martensite lath boundary, E_B is 40 kJ/mol and $\sigma_H V_H$ is 9–30 kJ/mol for σ_H ~ 4-15 GPa. From Eq. 3, the $C_{H\text{-}FPZ\ trap}$ is $6\text{x}10^6$ C_l. The lattice solubility (C_l) of H in AerMet®100 is unknown, but is $3\text{x}10^{-4}$ wppm for pure Fe exposed to 100 kPa H_2 at 298K [23]. This environment produces a hydrogen

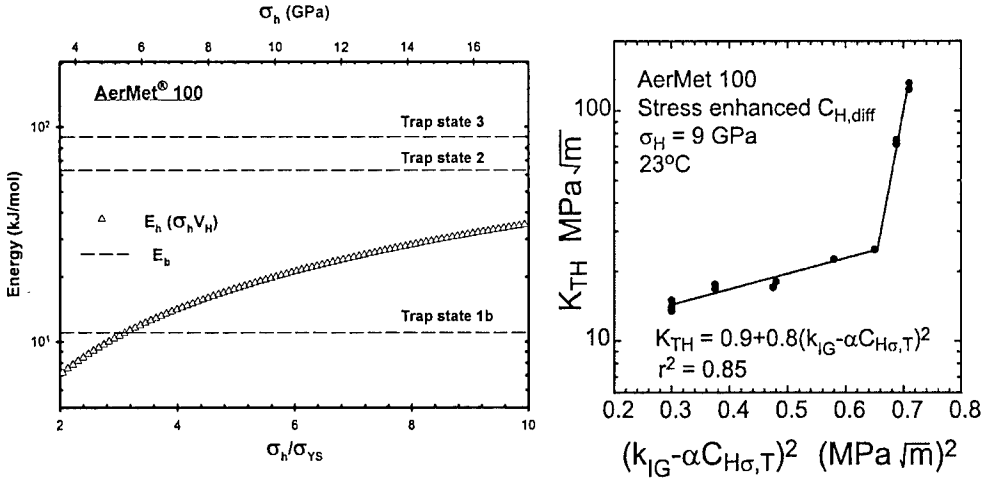

Figure 12. Left: The interaction energy $E_H = \sigma_h V_H$ *vs.* hydrostatic stress ahead of the crack tip compared with E_B for major trap states in aged ultra-high strength alloy steel [23]. Right: Measured and modeled effects of trapping + stress enhanced H concentration $C_{H\sigma,T}$ (or $C_{\text{H-Diff trap}}$ in Eq. 3) on the threshold for IHAC. $K_{TH} < 30$ MPa$\sqrt{m}$ relates to brittle, transgranular cracking, while fracture at higher K_{TH} involved some microvoid fracture [22]. σ_h in this plot is denoted as σ_H in the text.

fugacity equivalent to electrochemical charging at $\eta_{chg} = 0.0$ V and hence equals the lattice solubility for Fe precharged in $Ca(OH)_2$ at zero overpotential [22]. Using this estimate of C_l, $C_{H\text{-}FPZ\ trap}$ is on the order of 1600 wppm (9 atom pct) at 23°C. The effect of increasing H concentration in reducing the threshold for IHAC is predicted by coupling this trap and stress enhanced crack tip H content with a cracking model first developed to predict the temperature dependence of the macroscopic fracture toughness for cleavage, then extended to predict the yield strength, temperature and H concentration dependencies of K_{TH} [33]. Crack tip fracture is governed by the intrinsic Griffith toughness, k_{IG}, for cleavage fracture without H ($G_C \sim \gamma_S \sim k_{IG}^2/E$), where E is elastic modulus and γ_S is the energy required to produce unit crack surface. The local toughness is assumed to be reduced by H, yielding a Griffith-type threshold stress intensity for hydrogen embrittlement, k_{IH}, that equals ($k_{IG} - \alpha\ C_{\text{H-Diff trap}}$) where α is a coefficient and $C_{\text{H-Diff trap}}$ is enhanced according to Eq. 3. Local k_{IG} and k_{IH} were connected to macroscopic K_{IC} and K_{TH} using the super dislocation model of the crack tip discussed in conjunction with Fig. 11. The model predicts:

$$K_{TH} = \frac{1}{\beta'_{IHE}} \exp\left[\frac{\left(k_{IG} - \alpha C_{H-FPZ\,trap}\right)^2}{\alpha'' \sigma_Y}\right] \tag{4}$$

The parameters β'_{IHE} and α'' are constants determined by computer simulation of the dislocation structure about the crack tip. Comparison of theory and experiment is shown in Fig. 12 (right) [23]. Two parameters reported for Fe-Si ($k_{IG} = 0.85$ MPa$\sqrt{m}$ and $\alpha = 0.5$ MPa$\sqrt{m}$/atom fraction H [33]) were used to calculate the concentration term in Eq. 4 and plotted in Fig. 12. The fit to these IHAC data yielded values of β'_{IHE}

(0.13 *vs.* 0.2 $(MPa\sqrt{m})^{-1}$) and α'' ($3x10^{-4}$ *vs.* $2x10^{-4}$ MPa·m) essentially equal to those that fit measured K_{TH} *vs.* H_2 pressure and temperature for HEAC of a high strength steel [33]. These results suggest that modern formulations of high crack tip stresses are reasonable and necessary for next generation models of hydrogen embrittlement. Substantial crack tip H enhancement is supported quantitatively. There are, however, uncertainties in the details of such formulations, as well as in the additional amount of H produced by novel crack tip electrochemical reactions for HEAC compared to the more well defined total-dissolved H operative in IHAC.

5.1.2 Electrochemical Production of Crack Surface H

During HEAC, H may enrich by electrochemical and chemical reactions on crack tip surfaces. Experimental evidence is limited owing to the strong gradient of H penetration into the fracture process zone, localized over a 0.1-1 μm length scale as inferred from diffusion modeling discussed in Section 4. Several studies using secondary ion mass and quadrupole mass spectroscopies showed H uptake during stressed environmental exposure of Ni and Al alloys [51-53], however, these studies lacked spatial resolution and were not designed to measure crack tip H concentration.

Recent results demonstrate substantial H uptake and a new path to probe crack tip H enrichment. Thermal desorption spectroscopy (TDS) measurements of trapped H were performed on thinned specimens (~1 mm thick) machined inward from the wake surface of an HEAC crack in the aluminum alloy represented in Fig. 7. The measured amounts of H correlated with da/dt_{II} that depended on applied electrode potential and aging variables [14,30]. Levels of TDS-measured H were unexpectedly high since the FPZ is of order 0.1% of TDS specimen thickness and dilution should reduce H concentration to below TDS resolution. The obvious explanation is that H was enriched intensely in immediate proximity to the crack surface. This speculation was proved by Nuclear Reaction Analysis (NRA) applied to aluminum alloy specimens frozen in liquid nitrogen immediately after removal from stressed exposure in acidified-chloride solution at 23°C [14] or water vapor saturated air at 50-90°C [54]. In each environment, a high concentration of H was localized within 1 μm of the crack wake surface. A typical NRA measurement is presented in Fig. 13 [14], showing high H enrichment (~0.5 atom pct H) within 1 μm of the crack surface for the chloride solution case with 3 separate specimens and crack wake locations. Similar measurements were obtained for specimens cracked in hot water vapor, with up to 50 atom pct H, and experiments, confirmed that such H enrichment was not an artifact of the NRA method [54]. The H profiles in Fig. 13 are only reasonable if H diffuses slowly in aluminum, with $D_{H\text{-}eff} \sim 10^{-13}$ to 10^{-14} cm^2/s, several orders of magnitude less than reported [54]. This behavior is consistent with H trapping at vacancies injected into the crack wake lattice during metal oxidation [55-57]. Intense H enrichment in a micrometer sized crack tip volume, and the role of vacancies, are consistent with the results of the diffusion analysis discussed in conjunction with Fig. 9.

5.2 High Resolution Probes of Crack Tip Hydrogen Damage

New nano and micro-scale characterization methods must be applied to understand mechanisms of IHAC and HEAC. Fracture surface observation by scanning electron microscopy (SEM) has been used for decades to distinguish features suggestive of decohesion and plasticity damage [5,8,9]. For example, the presence of small voids on

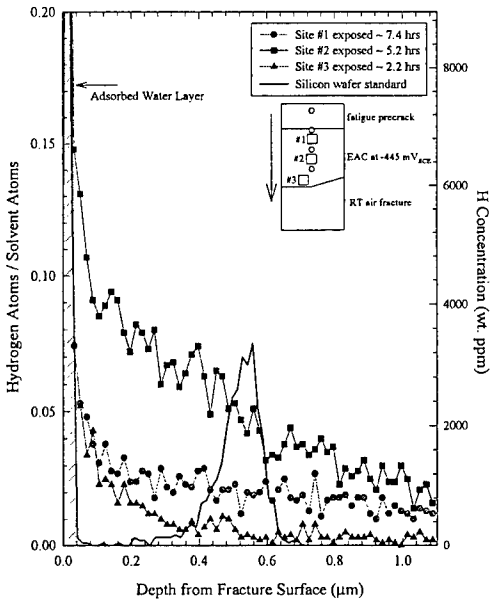

Figure 13. Nuclear reaction analysis of crack surface H accumulated during HEAC of 7075-T651 stressed quasi-statically in aqueous chloride solution at 23°C. Specimens were sectioned after testing, at 3 locations behind the crack tip and stored chilled. The solid line without data points measures H implanted precisely in a Si standard for calibration [14].

intergranular facets from HEAC suggests a strong role of H-enhanced plasticity and strain localization, but results are controversial. The argument that small-shallow voids are only resolved by careful transmission electron microscopy of shadowed replicas viewed at high tilt was reasonable [58], but modern SEM methods provide a means to test this concept. An example is summarized in Fig. 14, where an IG facet from HEAC in α hardened β-Ti (see Fig. 3) was examined with a high brightness electron source, multiple detectors to change surface topography, high magnification, and matching surface stereographic analysis [21,59]. Shallow microvoids as small as 0.02-0.04 μm in diameter should be resolved with this method; however, there was no evidence of an organized surface structure indicative of such voids. Rather, the features were undulations with occasional matching ridges and protrusion-cavity pairs, consistent with decohesion of β-Ti grain boundaries impacted by α precipitates in the underlying microstructure. Such a facet morphology does not prove decohesion, but provides evidence of the lack of structure manifest from H-sensitive slip band localization or microvoid formation during HEAC.

As a second example, transgranular cracking is prevalent in HEAC of aluminum alloys subjected to cyclic loading, and the crystallographic characteristics of fatigue crack surface features have important mechanistic implications [6,7]. Cracking is often along facet surfaces that are possibly parallel to {111} slip planes for inert environment plasticity driven damage, but shift to a {100} or {110} orientation when cyclic deformation occurs in the presence of crack tip H production from environmental reaction. It is important to characterize these features with sub-micrometer spatial

resolution to understand and model the physics of H damage. Ro reviewed methods employed to characterize crack facet surface crystallographic orientation [60]. He concluded that a combined Electron Back Scattered Diffraction (EBSD) analysis of grain orientation and stereological determination of vectors normal to facet surfaces in each oriented grain, provides the optimal approach to this problem [61]. This method is well suited to examine crack features in fine-grain size microstructures typical of commercial alloys. The method probes a large area of cracking, and sample preparation and alignment are relatively simple in comparison with other techniques. Modern scanning electron microscopes provide automated orientation determination by EBSD. The small probe size, combined with high resolution, provide the capability to analyze small elements of complex fatigue crack surfaces.

An example result from this method is presented in Fig. 15 for an Al-Li-Cu alloy stressed cyclically in ultra-high vacuum or two environments that produce H at the crack tip leading to fatigue by HEAC [60]. The SEM image (top) shows the fatigue crack surface morphology for water vapor and the intersecting metallographically

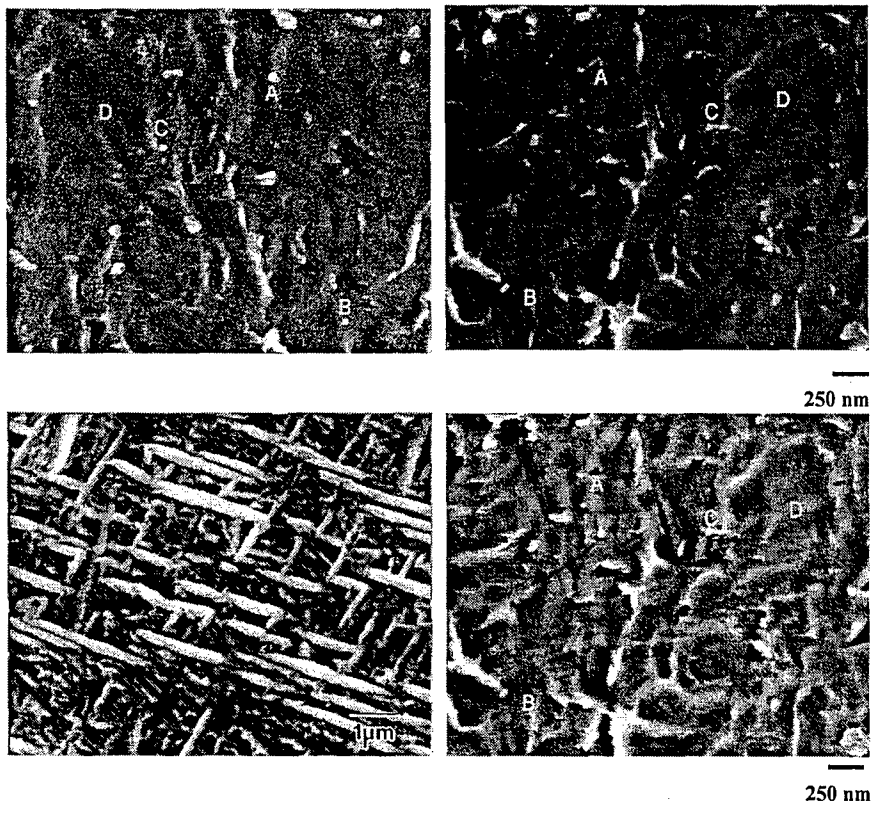

Figure 14. Matching field emission SEM images of an IG facet in α-hardened β-Ti cracked in aqueous NaCl following the conditions illustrated in Fig. 3. These high magnification images were formed with the signal accumulated from: (top left and right) the secondary electron detector immediately above the specimen, and (bottom right) dual secondary electron detectors and signal averaging. These top left-right two images were obtained from the matching-opposite areas of the fracture surface. Features A, B, and C are matching protrusion/cavity pairs; D shows subtle undulations on the fracture surface. The underlying microstructure is shown in the SEM back-scattered SEM image (bottom left) [21,59].

prepared plane with EBSD imaging of grain orientation. The stereographic triangles summarize the relationship between measured normals to crack facets and the orientation of the underlying grain structure. For vacuum, fatigue crack facets are essentially parallel to {111} slip planes, as expected given that this alloy is prone to slip band formation caused by shearable Al_3Li strengthening precipitates [61]. For fatigue in moist environments, the crack facet appearance is dramatically different from vacuum; the typical morphology is shown by the SEM fractograph. These facets were not predominantly parallel to low index planes, as simply hypothesized based on H-enhanced cleavage-like cracking for fatigue loading [7,61]. Rather, crack facets assume all orientations between {100} and {110}. This result was first reported for a different Al-Li-Cu-Zr alloy, based on manually determined and lower resolution EBSD/stereology [61].

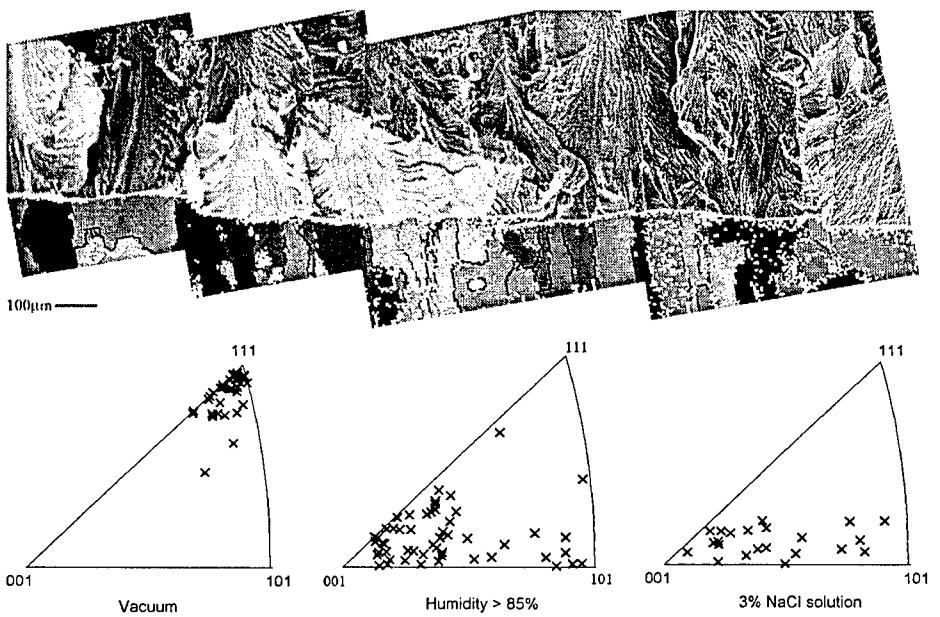

Figure 15. Crystallographic orientations of fatigue crack surface facets, determined by combined EBSD and stereological analyses, for an Al-2.5Cu-1.6Li-0.6Zn-0.08Zr alloy stressed cyclically in ultra-high vacuum and two environments that produce crack tip surface H that enhances fatigue crack propagation. The SEM fractograph and intersecting metallographic section, with superimposed orientation imaging map, are shown in the top image for fatigue cracking in moist air [60].

There are two mechanistic implications from the results in Fig. 15. For an alloy prone to slip band cracking in vacuum, H produces a sharp transition from slip based damage. If H-affected plasticity is critical to fatigue, then {111}-based cracking should be exacerbated, not eliminated. Second, facets observed for the moist environments assumed a wide range of possible orientations, but always consistent with planes subjected to high levels of crack tip normal and hydrostatic stresses [60]. This is consistent with decohesion, but the irrational character of crack facets suggests that the

physics of the H effect is not simple lattice cleavage. A working hypothesis is that cyclic plastic deformation evolves a dislocation cell structure that traps H and provides a path of connected damage for cracking that is not always crystallographic [60]. This notion has not been probed experimentally. Transmission electron microscope examination of a crack wake thin foil prepared by focused ion beam machining is a new technique that should be used to establish such mechanisms of H cracking [62].

It is critical to use new experimental methods to calibrate and validate crack tip stress and strain distributions (Section 5.1.1), with emphasis on the strong gradients over 0.05-10 μm. Geometrically necessary dislocations change lattice orientation and may be detected by diffraction-based techniques. EBSD was applied to investigate local plasticity associated with cracking [63] and this technique should be exploited. Micro-Laue diffraction using focused synchrotron x-rays probes a material in 3 dimensions with spatial resolution of ~0.5 x 0.5 x 1.0 μm [64]. For aluminum, the maximum probe depth is ~75 μm. Work is ongoing to measure fatigue crack tip plasticity in aluminum alloys cracked in ultra-high vacuum or moist N_2 [65]. The experiment involves depth resolved synchrotron line scans perpendicular to the cracking direction and on a polished surface. Figure 16 shows how crack wake plasticity is manifest in a micro-Laue diffraction pattern. Undeformed material away from the crack produces sharp-intense spots (left image), while the region near the crack exhibits asterism (right image) characteristic of plasticity. Such results are connected with non-local plasticity models and the notion that geometrically necessary dislocations are responsible for hardening [66]. This extra dislocation content can be assessed and its impact on local flow stress predicted for use in crack tip mechanics models. This method is suitable to investigate the effects of dissolved H, grain microstructure/anisotropy, and ΔK level on crack tip plasticity. A specific issue being studied is differences in GND content for crack growth in vacuum compared to moist N_2 that produces substantial H dissolved in the zone about the crack tip.

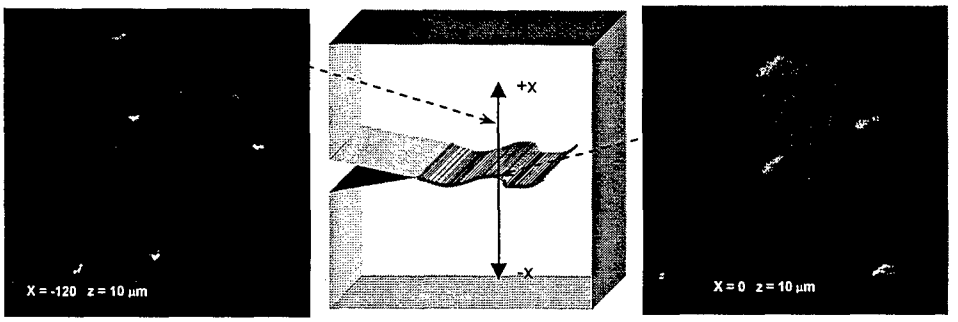

Figure 16. Micro-Laue diffraction patterns, obtained adjacent to (x = 0 μm, right image) and below (x = -120 μm, left image) the crack plane under (z = 10 μm) the surface, for a vacuum fatigue crack in a specimen of the Al-Li alloy represented in Fig. 15 [65].

5.3 Effect of Active Strain Rate on Hydrogen Embrittlement

It is well known that IHAC and HEAC are promoted by loading formats that produce active crack tip strain rates in excess of the level from quasi-static loading and slow

crack growth, with the effect particularly significant in lower strength alloys [5]. Considering HEAC, crack tip strain rate is a dominant factor for alloys that form a crack tip passive film concurrent with H production [19,24,28]. In this case H production and uptake are promoted if crack tip strain rate is sufficient to repeatedly fracture the passive film, perhaps at sites where active slip bands intersect the reacting crack tip surface [67]. Based on this mechanism, the rising-CMOD (crack mouth opening displacement) test provides an effective method to characterize alloy resistance to HEAC and can promote cracking that is not otherwise caused by quasi-static K loading [5]; typical results are shown in Figs. 3 and 6.

The effect of crack tip strain rate is strong for IHAC of low to moderate strength steels, as illustrated in Fig. 17 for a bainitic Cr-Mo steel, precharged with H by exposure to high temperature and pressure H_2 then loaded in moist air at 23°C [68,69]. The threshold stress intensity for crack arrest at fixed CMOD (and decreasing K) increases dramatically with declining steel yield strength for a constant-dissolved H content. This is well known behavior [5]. In sharp contrast, the threshold K for the onset of subcritical H cracking under rising CMOD (and rising K) is constant or declines mildly with decreasing σ_{YS}. Since crack tip strain rate depends much more strongly on dK/dt than da/dt [19], Fig. 17 suggests that IHAC is exacerbated greatly by higher crack tip strain rate but only for the lower strength regime.

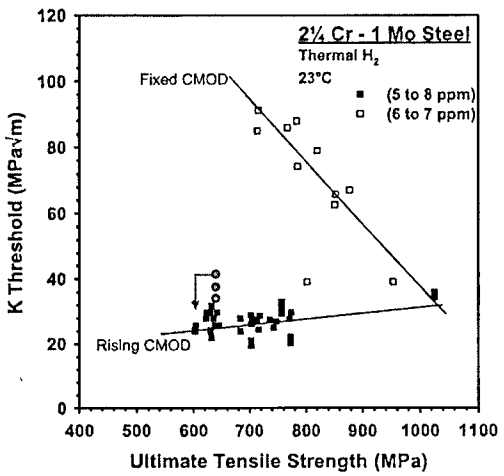

Figure 17. The effect of loading format, including fixed CMOD crack arrest (open) and rising CMOD causing crack growth initiation (filled), on IHAC of a tempered bainitic alloy steel containing H precharged from either bulk-H_2 exposure at elevated temperature (9, □) or active electrochemical charging on a slot surface remote from the crack tip (♦) [68-70].

The mechanism for the effect of crack tip strain rate on IHAC is not well defined. A first step is to demonstrate that this response is not an artifact of H loss from the precharged specimen and during the long testing time typical of crack arrest at fixed CMOD. A new method was developed to eliminate H loss using the slotted and fatigue precracked compact tension specimen shown in Fig. 18. Hydrogen is precharged from electrochemical reactions limited to the slot surfaces, before loading and continuously during rising CMOD loading, to provide a fixed H flux incoming to the crack tip without crack tip electrolyte exposure and complicating HEAC. The necessary elastic-plastic J integral, elastic stress intensity, and elastic compliance solutions, as well as 3-dimensional H diffusion modeling by finite elements, were developed to analyze the threshold and kinetics of IHAC in the slotted specimen [70]. Severe H cracking was

produced with this method applied to temper embrittled Cr-Mo weld metal, as indicated by (♦) in Fig. 17 [70]. The threshold is substantially lower than K_{IC} for this steel (~120 MPa$\sqrt{m}$), but somewhat higher than the standard specimen results in Fig. 17 because the high H content produced by H_2 exposure at elevated temperature (5-8 wppm) was not achieved by electrochemical charging that yielded 3 wppm H at best [70].

The slotted specimen test method showed that applied CMOD exacerbated H

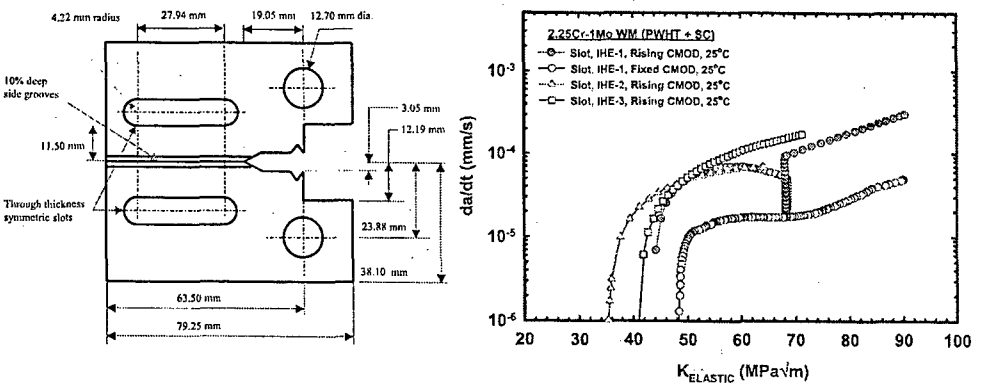

Figure 18. Left: The slot-modified compact tension specimen. Right: Crack growth rate *vs.* applied K for Cr-Mo steel weld metal loaded in moist air at 23°C, concurrent with H charging from a sulfuric acid-thiosulfate electrolyte and cathodic polarization in contact with the slot surfaces but isolated from the crack tip [70].

cracking. If loading was stopped after IHAC initiated, crack growth rate immediately declined. This behavior is shown in Fig. 18 where 3 replicate da/dt *vs.* K results for rising CMOD exceed the growth rates measured for fixed CMOD. For the former, K rises with subcritical crack growth, but K falls for the fixed CMOD crack arrest condition. Where CMOD was fixed during rising CMOD, crack growth slowed to the quasi-static fixed CMOD result. A single da/dt *vs.* K relationship was not observed for these different loading formats, attesting to the effect of crack tip strain rate for constant H flux to the crack tip. Additional experiments showed that da/dt is directly proportional to dK/dt, and furthermore, this severe IHAC is eliminated as test temperature increased above 50°C [70]. This temperature effect is well known for H cracking in high strength alloys [5], but this is the first demonstration of such behavior where H loss from bulk precharging is precluded.

The crack tip damage mechanism for the IHAC behavior indicated in Figs. 17 and 18 most likely involves interaction of H trapping and plasticity. The finite element calculated amount of H, delivered to the crack tip FPZ from H_2 or slot charging and including the enriching effects of microstructural trapping and crack tip hydrostatic stress (Eq. 3), correlates the effects of bulk H level and temperature on threshold [70].

6.0 Conclusions

- Modern strong-tough alloys suffer severe H cracking, similar to older materials and limiting structural applications. Transgranular cracking modes are

particularly important, but precise microstructural causes are not understood sufficiently to enable H-cracking resistant alloy development.

- H-cracking limits alloy performance for both monotonic and cyclic loading, and similar crack tip damage mechanism and modeling approaches are valid.
- Micromechanical models of crack tip conditions predict important trends in threshold and subcritical crack growth rate behaviour for IHAC and HEAC. H diffusion appears to rate limit da/dt and da/dN for monotonic and cyclic loading, however, uncertain-adjustable parameters limit model effectiveness.
- Nano-mechanics modeling and experimental results show high levels of H accumulated in the crack tip fracture process zone, as necessary for decohesion. Contributing mechanisms include high crack tip stresses due to localized dislocation-based processes such as gradient plasticity, as well as powerful H production and trapping proximate to electrochemically reacting crack surfaces.
- New sub-micrometer resolution probes of crack tip damage will better define features such as crack path crystallography (EBSD + Stereology) and surface morphology (high brightness, dual detector SEM), local H concentration (TDS and NRA), and will validate crack tip mechanics modelling (micro-Laue x-ray diffraction and EBSD).
- Active crack tip strain rate exacerbates H-cracking, particularly in low to moderate strength alloys. A new method shows that IHAC is governed by intrinsic H-plasticity interaction rather than H loss during loading.

7.0 Acknowledgements

Preparation of this review was supported by the Office of Naval Research (Grant N000-111-222), with Dr. Airan Perez as Scientific Officer. Professors S.R. Agnew, M.R. Begley, R.G. Kelly, and J.R. Scully provided important insights and collaborations throughout this work. These contributions are gratefully acknowledged.

8.0 References

[1] R.W. Staehle, et al. (Eds.) Stress Corrosion Cracking and Hydrogen Embrittlement of Iron Base Alloys, NACE, Houston, TX, 1977.

[2] R.P. Gangloff and M.B. Ives (Eds.) Environment Induced Cracking of Metals, NACE, Houston, TX, 1990.

[3] N.R. Moody et al. (Eds.) Hydrogen Effects on Material Behavior and Corrosion Deformation Interactions, Minerals, Metals & Materials Society, Warrendale, PA, 2003.

[4] P. Sofronis (Ed.) Engr. Frac. Mech. 68, 2001.

[5] R.P. Gangloff, in: I. Milne, R.O. Ritchie and B. Karihaloo (Eds.) Comprehensive Structural Integrity, Vol. 6, Elsevier Science, New York, NY, 2003, pp. 31-101.

[6] R.P. Gangloff, in: R.P. Gangloff and M.B. Ives (Eds.) Environment Induced Cracking of Metals, NACE, Houston, TX, 1990, pp. 55-109.

[7] R.P. Gangloff, in: Fatigue 02, Anders Blom (Ed.) Engineering Materials Advisory Services, West Midlands, UK, 2002, 3401-3433.

[8] S.P. Lynch, in: N.R. Moody et al. (Eds.) Hydrogen Effects on Material Behavior and Corrosion Deformation Interactions, Minerals, Metals & Materials Society, Warrendale, PA, 2003, 449-466.

[41] W.W. Gerberich, R.A. Oriani, M.J. Lii, X. Chen, and T. Foecke, Phil. Mag. A 63 (1991) 363-376.
[42] X. Chen and W.W. Gerberich, Metall. Trans. A 22A (1991) 59-70.
[43] D.M. Lipkin, D.L. Clarke, and B. Beltz, Acta Mater., 44 (1996) 4051-4058.
[44] M.R. Begley, S.R. Agnew, U. Komaragiri, and R.P. Gangloff, "Hydrogen Damage in the Crack Tip Environment", in: A. Carpinteri et al. (Eds.) Proceedings, International Congress on Fracture-11, Elsevier Science, Oxford, UK, (2004).
[45] A. Needleman and J.G. Sevillano, Scripta Mater, 48 (2003) 109-111.
[46] N.A. Fleck and J.W. Hutchinson, in: J.W. Hutchinson and T.Y. Wu (Eds.) Advances in Applied Mechanics, Vol. 33, Academic Press, NY, 1992, 295-361.
[47] H. Jiang, Y. Huang, Z. Zhuang and K.C. Hwang, J. Mech. Phys. Solids., 49 (2001) 979-993.
[48] H.M.M. Cleveringa, E. Van der Giessen, and A. Needleman, J. Mech. Phys. Solids 48 (2000) 1133-1157.
[49] T.Y. Zhang and J.E. Hack, Metall. Mater. Trans. A 30A (1999) 155-159.
[50] T.Y. Zhang, H. Sheu, and J.E. Hack, Scripta Metall. Mater 27 (1992) 1605-1610.
[51] J. Okahana, S. Kuramoto and M. Kanno, in: N.R. Moody et al. (Eds.) Hydrogen Effects on Material Behavior and Corrosion Deformation Interactions, Minerals, Metals & Materials Society, Warrendale, PA, 2003, 909-917.
[52] P. Rozenak, E. Siros, I.M. Robertson, and H.K. Birnbaum, Isr. J. Technol. 24 (1988) 183-189.
[53] B. Ladna and H.K. Birnbaum, Acta Metall. 35 (1987) 2537-2542.
[54] G.A. Young and J.R. Scully, in: N.R. Moody et al. (Eds.) Hydrogen Effects on Material Behavior and Corrosion Deformation Interactions, Minerals, Metals & Materials Society, Warrendale, PA, 2003, 893-907.
[55] C.E. Buckley and H.K. Birnbaum, Physica B 241-243 (1997) 344-346.
[56] H.K. Birnbaum, C. Buckley, F. Zeides, E. Sirois, P. Rozenak, S. Spooner, and J.S. Lin, J. Alloys and Compounds 253-254 (1997) 260-264.
[57] R.B. McLellan and D. Zang, Acta Mater. 49 (2001) 377-387.
[58] S.P. Lynch, in: P.R. Swann, F.P. Ford, and A.R.C. Westwood (Eds.) Mechanisms of Environment Sensitive Fracture of Materials, Metals Society, London, UK, 1977, 201-212.
[59] B.P. Somerday, Metallurgical and Crack-Tip Mechanics Effects on Environment-Assisted Cracking of Beta-Titanium Alloys in Aqueous Chloride, PhD Dissertation, University of Virginia, Charlottesville, VA, 1998.
[60] Yunjo Ro, Fatigue Crack Surface Crystallography of Precipitation Hardened Aluminum Alloys, MS Thesis, University of Virginia, Charlottesville, VA, 2004.
[61] D.C. Slavik and R.P. Gangloff, Acta Metall. Mater. 44 (1996) 3515-3534.
[62] S.M. Kazanjian, Fatigue Deformation in Beta Titanium Ti-15V-3Al-3Sn-3Cr, Ph.D. Dissertation, University of Virginia, Charlottesville, VA, 2004.
[63] L.N. Brewer, M.A. Othon, L.M. Young, and T.M. Angeliu, Microscopy and Microanalysis 8 (2002) 684CD ~ 685CD.
[64] B.C. Larson, W. Yang, G.E. Ice, J.D. Budai, and J.Z. Tischler, Nature. 415 (2002) 887-890
[65] S.R. Agnew, Y.J. Ro, M.R. Begley, and R.P. Gangloff, "Fatigue Crack Tip Damage-Based Models in Structural Prognosis", in: A. Carpinteri et al. (Eds.) Proceedings, International Congress on Fracture-11, Elsevier Science, Oxford, UK, 2004.
[66] C.S. Hartley, TMS Lett. 1 (2004) 11-12.
[67] D.G. Kolman and J.R. Scully, Phil. Mag. A 79 (1999) 2313-2338.
[68] R.P. Gangloff, in: M. Levy and S. Isserow (Eds.) Corrosion Prevention and Control, US Army Laboratory Command, Watertown, MA, 1986, 64-111.
[69] R.P. Gangloff, B.P. Somerday and D.L. Cooke, in: P.L. Andresen and R.N. Parkins (Eds.) Life Prediction of Structures Subject to Environmental Degradation, NACE, Houston, TX, 1996, 161-175.
[70] A.M. Al-Rumaih, Measurement and Modeling of Temperature Dependent Hydrogen Embrittlement of Cr-Mo Steel to Enable Fitness-for-Service Modeling, PhD Dissertation, University of Virginia, Charlottesville, VA, 2004.

[9] H.K. Birnbaum, I.M. Robertson, P. Sofronis and D. Teter, in: T. Magnin (Ed.) 2nd International Conference on Corrosion-Deformation Interactions, Institute of Materials, London, UK, 1997, pp. 172-195.
[10] C.J. McMahon, Jr., Engr. Frac. Mech. 68 (2001) 773-788.
[11] R.A. Oriani, in: R.P. Gangloff and M.B. Ives (Eds.) Environment Induced Cracking of Metals, NACE, Houston, TX, 1990, 439-448.
[12] J.A. Lillard, Environment Assisted Cracking of a Nickel-Based Superalloy in Hydrogen-Producing Solutions, PhD Dissertation, University of Virginia, Charlottesville, VA, 1998.
[13] N.R. Moody, M.W. Perra and S.L. Robinson, Scripta Metall. 22 (1988) 1261-1266.
[14] K.R. Cooper, L.M. Young, R.P. Gangloff, and R.G. Kelly, Matls. Sci. For. 331-337 (2000) 1625-1634.
[15] A. Turnbull, Corrosion, 57 (2001) 175-189.
[16] S.P. Lynch, in: This proceedings, 2004.
[17] G.B. Olson, Advanced Matls. Proc. July (1997) 72-79.
[18] B.P. Somerday and R.P. Gangloff, Matls. Sci. Engr. A254 (1998) 166-178.
[19] B.P. Somerday, L.M. Young and R.P. Gangloff, Fatg. Fract. Engr. Matls. Struct. 23 (2000) 39-58.
[20] S.P. Hayes, Internal Hydrogen Embrittlement of High Strength Beta-Alpha Titanium Alloys, PhD Dissertation, University of Virginia, Charlottesville, VA, 2000.
[21] B.P. Somerday, A.W. Wilson, J.M. Howe, and R.P. Gangloff, Microstructural Cause of Intergranular Hydrogen Environment Embrittlement of Aged Beta-titanium Alloys. Unpublished research, University of Virginia, Charlottesville, VA, 2004.
[22] R.L.S. Thomas, J.R. Scully and R.P. Gangloff, Metall. Mater. Trans., A 34A (2003) 327-344.
[23] D. Li, R.P. Gangloff, and J.R. Scully, Metall. Mater. Trans., A 35A (2004) 849-864.
[24] E. Richey, III and R.P. Gangloff, in R.D. Kane (Ed.) Environmentally Assisted Cracking, STP 1401, ASTM International, West Conshohocken, PA, 2000, 104-127.
[25] L.M. Young and R.P. Gangloff, in: M. Tiryakioglu (Ed.) Advances in the Metallurgy of Aluminum Alloys, ASM International, Materials Park, OH, 2001, 135-140.
[26] M.F Blackburn and J.C. Williams, Trans. ASM 62 (1969) 398-409.
[27] H.G. Nelson, in: I.M. Bernstein and A.W. Thompson (Eds.) Hydrogen in Metals, ASM International, Materials Park, OH, 1974, 445-464.
[28] E. Richey, III, Microstructure and Strain Rate Effects on the Environment Assisted Cracking of α/β-Ti Alloys in Aqueous Chloride, PhD Dissertation, University of Virginia, Charlottesville, VA, 2000.
[29] N.J.H. Holroyd, in: R.P. Gangloff and M.B. Ives (Eds.) Environment-Induced Cracking of Metals, NACE, Houston, TX, 1990, 311-345.
[30] L.M. Young, Microstructural Dependence of Aqueous-Environment Assisted Crack Growth and Hydrogen Uptake in AA7050, PhD Dissertation, University of Virginia, Charlottesville, VA, 1999.
[31] J.M. Barsom and S.T. Rolfe, Fracture and Fatigue Control in Structures, 2nd Ed., Prentice-Hall, Englewood Cliffs, NJ, 1987.
[32] R.P. Wei and D.G. Harlow, in: This proceedings, 2004.
[33] W.W. Gerberich, P.G. Marsh and J.W. Hoehn, in: A.W. Thompson and N.R. Moody (Eds.) Hydrogen Effects in Materials, Minerals, Metals & Materials Society, Warrendale, PA, 1996, 539-553.
[34] Y. Katz, N. Tymiak and W.W. Gerberich, Engr. Frac. Mech. 68 (2001) 619-646.
[35] R.P. Gangloff, in: N.R. Moody et al. (Eds.) Hydrogen Effects on Material Behavior and Corrosion Deformation Interactions, Minerals, Metals & Materials Society, Warrendale, PA, 2003, 477-497.
[36] Z. Gasem and R.P. Gangloff, in: R.H. Jones (Ed.) Chemistry and Electrochemistry of Corrosion and Stress Corrosion Cracking, Minerals, Metals & Materials Society, Warrendale, PA, 2001, 501-521.
[37] R.P. Wei and R.P. Gangloff, in: R.P. Wei and R.P. Gangloff (Eds.) Fracture Mechanics: Perspectives and Directions, STP 1020, ASTM International, West Conshohocken, PA, 1989, 233-264.
[38] R.A. Oriani, *Annual Reviews in Materials Science*, 8 (1978) 327-357.
[39] R.P. Gangloff, Matls. Sci. Engr. A103 (1988) 157-166.
[40] J. Kameda, Acta Metall., 34 (1986) 867-882.